nature neuroscience

SUPPLEMENTARY INFORMATION

https://doi.org/10.1038/s41593-019-0364-9

In the format provided by the authors and unedited.

Expectation-induced modulation of metastable activity underlies faster coding of sensory stimuli

L. Mazzucato[1,2], G. La Camera[1,3]* and A. Fontanini[1,3]*

[1]Department of Neurobiology and Behavior, State University of New York at Stony Brook, Stony Brook, NY, USA. [2]Departments of Biology and Mathematics and Institute of Neuroscience, University of Oregon, Eugene, OR, USA. [3]Graduate Program in Neuroscience, State University of New York at Stony Brook, Stony Brook, NY, USA. *e-mail: giancarlo.lacamera@stonybrook.edu; alfredo.fontanini@stonybrook.edu

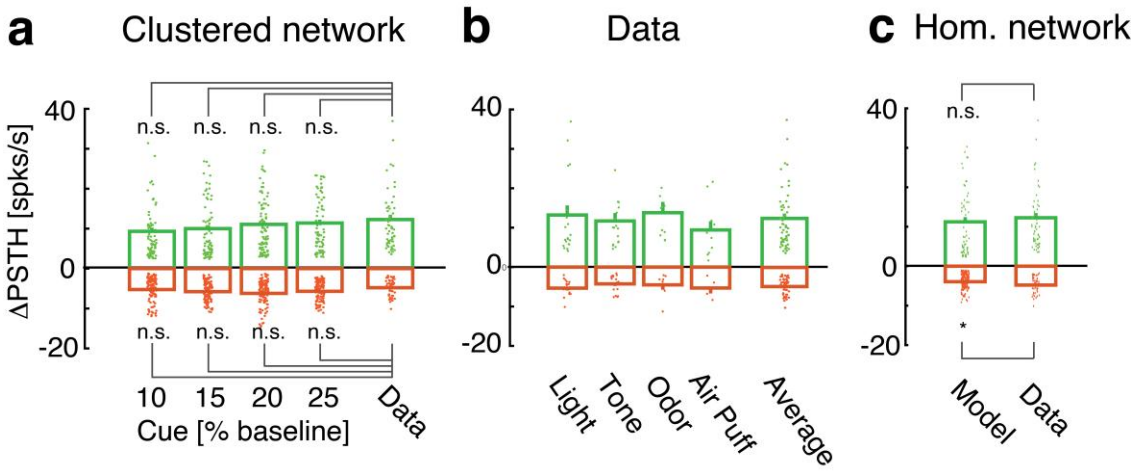

Supplementary Figure 1

Cue responses in data and model.

a: Comparison of cue responses of the clustered network with those published in Ref.[10] (right-most bar). Shown are the peak firing rate responses for different values of cue-induced spatial variance σ^2. **b:** Data from different sensory modalities together with across-modalities average in the rightmost bar from Ref.[10] **c**: same as **a** for the homogeneous network with $\sigma^2 = 20\%$. Peak responses (ΔPSTH, mean±s.e.m. across neurons from *n=20* simulated networks, 50 neurons/network were randomly sampled; dots represent single neurons) were computed as the difference between the peak activity post-cue and the average activity pre-cue. Single neuron responsiveness was defined via a change-point analysis (see Methods). In the data, PSTH modulation in cue-responsive neurons was consistent across modalities (excited responses peaked at 12 ± 1.0 spks/s, inhibited responses peaked at -4.8 ± 0.3 spks/s). In the model, cue responses depended only slightly on the cue-induced modulation of the spatial variance σ^2 (expressed in percent of baseline; see panel **a**), and were in quantitative agreement with the data over a wide range of parameters. When $\sigma = 20\%$, cue responses were: in the clustered network model (see Fig. 1a-c of the main text), 11.1 ± 0.8 spks/s (excited) and -6.2 ± 0.3 spks/s (inhibited); in the homogeneous network (panel **c**, see Fig. 1d-f of the main text), cue responses had average peaks 11.2 ± 1.2 spks/s (excited) and -3.9 ± 0.2 spks/s (inhibited, significantly different from Data, two-sided *t*-test, *p=0.04*). Panels **a** and **c**: two-sided *t*-test with multiple comparison Bonferroni correction, *=p<0.05; n.s.=non-significant. "Data" in panels **a** and **c** is the same as "Average" in panel **b**.

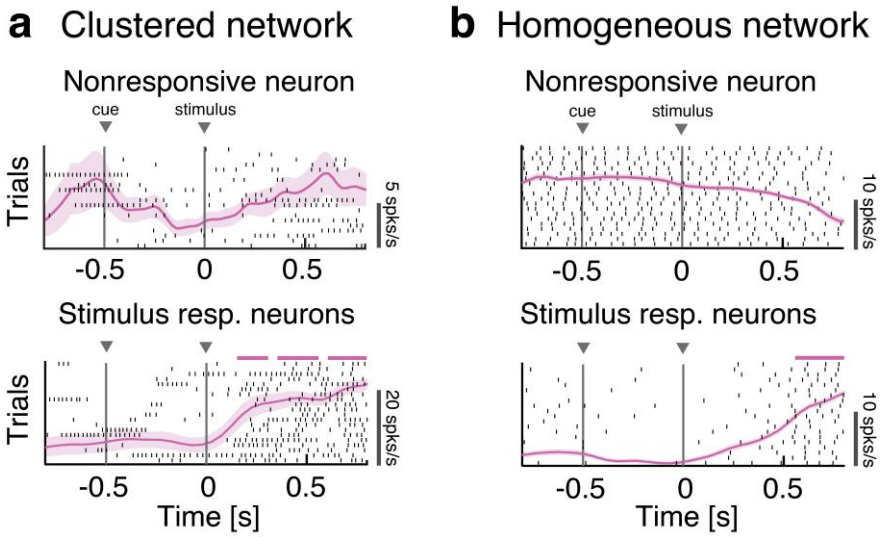

Supplementary Figure 2

Model neurons with no cue response.

Raster plots and PSTH (pin curves) of representative single neuron responses to cue and one stimulus in expected trials in the clustered (**a**) and homogeneous (**b**) networks. *Top row*: non-responsive neurons. *Bottom row*: neurons that are stimulus-responsive but not cue-responsive. A neuron was deemed responsive if the PSTH was significantly different from baseline (pink horizontal bars: $p<0.05$, two-sided t-test with multiple-bin Bonferroni correction). The PSTHs report mean±s.e.m. firing rate across 20 simulated trials with the same stimulus.

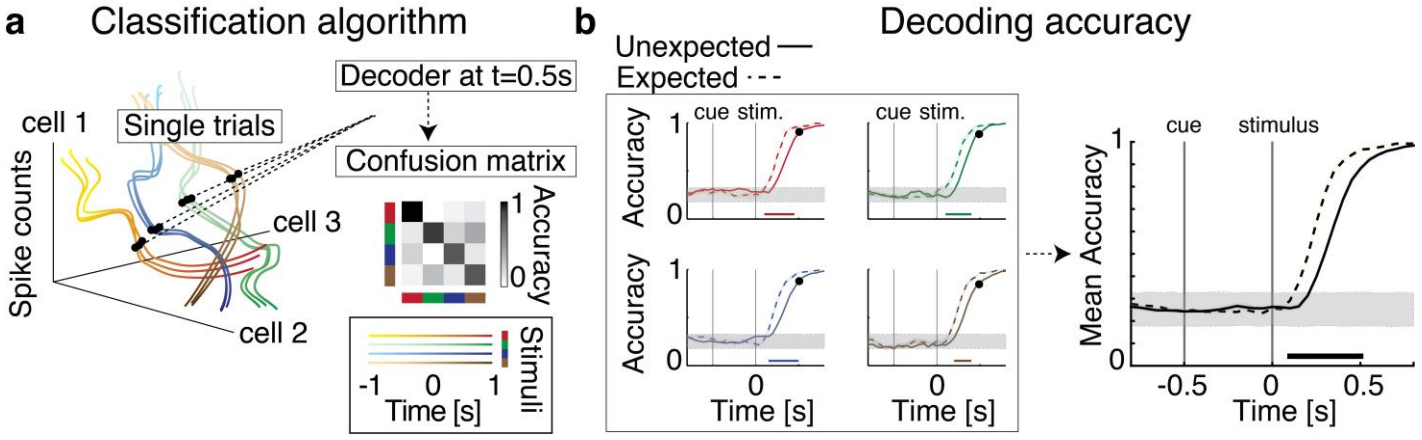

Supplementary Figure 3

Classification algorithm used for population decoding.

a: Stimulus decoding is accelerated in the presence of the anticipatory cue. Here we show that similar results are obtained when considering the decoding accuracy for single tastes separately. **a**: Schematics of the decoding algorithm: The colored curves represent the temporal evolution of neural activity across N simultaneously recorded neurons. The four colors label trajectories obtained with four different stimuli (tastants). Hues help visualize the time course within each trajectory. Each time bin of activity (black dots) was decoded using an independent classifier. Within each condition ('expected' or 'unexpected'), decoding performance was assessed via a cross-validation procedure, yielding a confusion matrix whose diagonal represents the accuracy of classification for each taste in that time bin. **b**: Time course of decoding accuracy in expected (dashed curves) vs. unexpected (full curves) conditions for each individual tastant (left, color-coded) and for the across-taste average (right). The left panel demonstrates coding anticipation for each tastant separately. Color-coded horizontal bar represents significant difference between decoding accuracy in expected vs. unexpected trials, $p<0.05$, two-sided t-test with multiple bin Bonferroni correction (notations as in Fig. 1c of the main text).

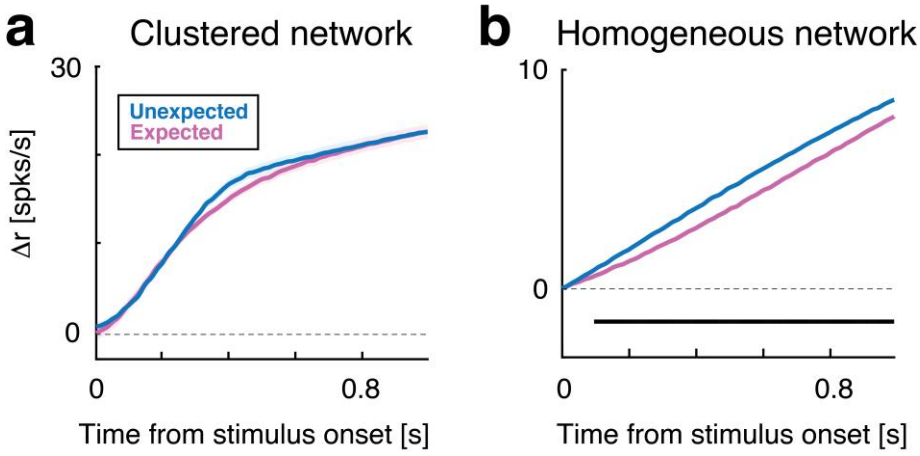

Supplementary Figure 4

Firing-rate coding of expectation.

Stimulus coding could accelerate if the cue increased the firing rate of the stimulus-selective neurons compared to the non-selective neurons. Here we show that coding anticipation in the clustered network is not driven by such cue-induced changes in firing rate selectivity. To prove this point, we estimated the time course of the firing rate difference Δr between stimulus-selective and nonselective neurons in the expected (pink) and unexpected (blue) conditions in the clustered and homogeneous networks. We found no difference in Δr between conditions in the clustered network (**a**), demonstrating that anticipatory activity is not driven by changes in firing rates. In the homogeneous network (**b**), Δr was larger in the unexpected condition, in agreement with the reversed trend in coding speed found in Fig. 1f. Panel **b**: black horizontal bar: $p<0.05$, two-sided *t*-test with multiple bin Bonferroni correction. Both panels: main curves represent means of Δr over 20 sessions; shaded area represents s.e.m.

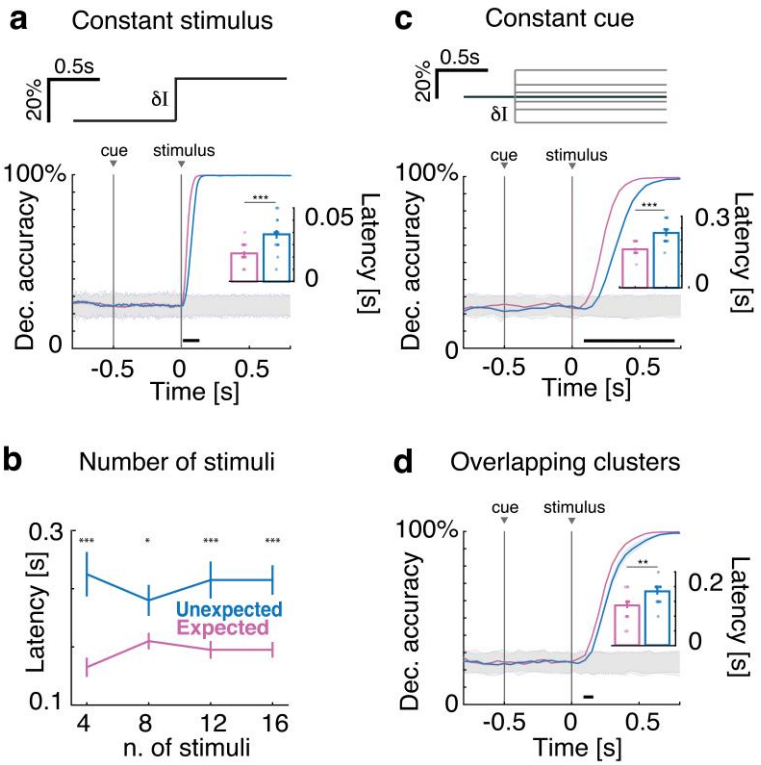

Supplementary Figure 5

Robustness of anticipatory activity.

a: Anticipatory activity is present in the case of step-like stimuli (top: time course of stimulus as a fraction of baseline afferent current; bottom: time course of decoding accuracy; notations as in Fig. 1c of main text). *Inset*: aggregate analysis across *n=20* simulated networks of the onset times of significant decoding (mean±s.e.m.) in expected (pink) vs. unexpected trials (blue) shows significantly faster onsets in the expected condition (two-sided t-test, $p=4.0\text{x}10^{-4}$). **b**: Anticipatory activity did not depend on the number of stimuli presented to the network. Latency of significant stimulus decoding was faster in expected (pink) compared to unexpected (blue) trials with up to 16 stimuli (clusters were selective to a given stimulus with 50% probability; error bars represent mean±s.e.m. across *n=20* simulated networks). **c**: Anticipatory activity was present in the case of step-like cue with spatial variance σ=20% and a linearly ramping stimulus as in main Fig. 2a (top: time course of stimulus as a fraction of baseline afferent current; inset notations as in panel **a**: two-sided t-test, $p=1.5\text{x}10^{-4}$). **d**: Anticipatory activity was present even with overlapping clusters[33]. In this model, neurons had a probability f=0.06 of belonging to one of the Q=14 clusters, with a fraction of $f^k(1-f)^{Q-k}$ neurons belonging to any set of k specific clusters and E-to-E synaptic connections given by $J_{ij} = p_{EE}(\epsilon_{ij}\xi_+ + (1-\epsilon_{ij})\xi_-)$. Here, p_{EE}=0.2 is the connection probability; $\xi_\pm$ are the synaptic weights values sampled from normal distributions with means $J_\pm$ and variances $\delta^2 J_\pm^2$, respectively (δ=0.01). The synaptic weights were potentiated with probability $\epsilon_{ij} = \frac{P_{ij}}{P_{ij}+\rho\, f D_{ij}}$, where $P_{ij} = \Sigma_{k=1}^{Q}\eta_i^k\eta_j^k$ is the number of clusters in common between neurons i and j ($\eta_i^k = 1$ if cluster k contains neuron i and $\eta_i^k = 0$ otherwise), while $D_{ij} = \Sigma_{k=1}^{Q}\eta_i^k(1-\eta_j^k)$, with ρ=2.75 (see Ref.[30] for more details on this model). The E-to-I, I-to-E, and I-to-I connection probability, the stimuli and the anticipatory cue were the same as for the clustered networks (Table 1 in the main text). The remaining parameters of the network are reported in Table S1 (inset notations as in panel **a**: two-sided t-test, $p=1.1\text{x}10^{-3}$). Main panels: *=p<0.05, **=p<0.01, ***=p<0.001, post-hoc *t*-test with Bonferroni correction. Horizontal black bar, p<0.05, two-sided *t*-test with multiple-bin Bonferroni correction. Insets: **=p<0.01, ***=p<0.001, two-sided *t*-test.

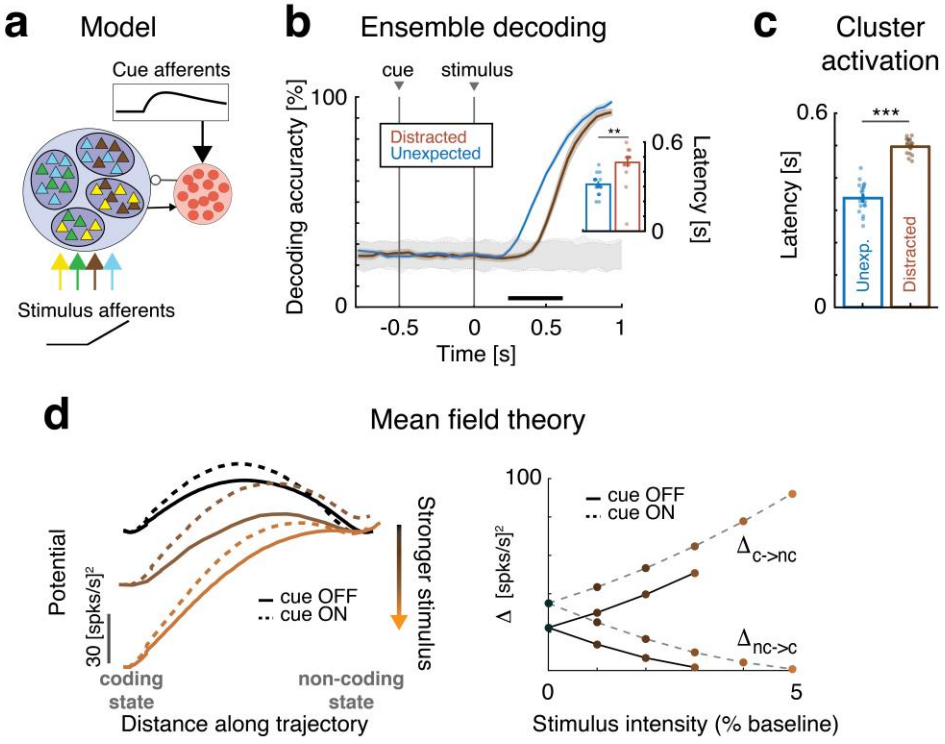

Supplementary Figure 6

A distracting cue slows down stimulus coding (model).

To show that the anticipatory effect of our model cue is specific, we give here an example of a manipulation leading to the opposite effect. Specifically, if the cue is modeled as an increase in the mean input current to the inhibitory population (we refer to such a cue as a "distractor"), stimulus decoding is slowed down rather than accelerated. As we show in the following panels, the coding delay following such "distracting cue" is the consequence of increased energy barriers (panel d) causing slower transition dynamics. In turn, this is due to the sharpening of the effective transfer functions of the excitatory neurons, reflecting increased stability induced by the increased inhibition. **a**: Schematics of clustered network architecture and stimulation (notations as in Fig. 1a of the main text, here the cue targets the inhibitory neurons). **b**: Time course of cross-validated decoding accuracy during distracted (brown) trials was slower than during unexpected (red) trials (notations as in Fig. 1c). Inset: aggregate analysis across $n=20$ simulated networks, mean±s.e.m.; two-sided t-test, $p=1.3\text{x}10^{-3}$). **c**: Activation latency of stimulus-selective clusters after stimulus presentation was delayed during distracted trials (mean±s.e.m. across $n=20$ simulated networks, two-sided t-test, $p=1.5\text{x}10^{-13}$). **d**: Mean field theory of simplified 2-cluster network (notations and model as in Fig. 4c, lighter brown denotes stronger stimuli). *Left panel*: the transition probability from the non-coding (right well) to the coding state (left well) increased with larger stimuli. In 'distracted trials' (dashed curves) the barrier height Δ from the non-coding to the coding state is larger than in unexpected trials (full curves), leading to slower coding in the distracted condition. *Right panel*: effective energy barriers as a function of stimulus intensity, with (full lines) and without the cue (dashed). Panels **b** and **c**: **=p<0.01, ***=p<0.001, two-sided t-test.

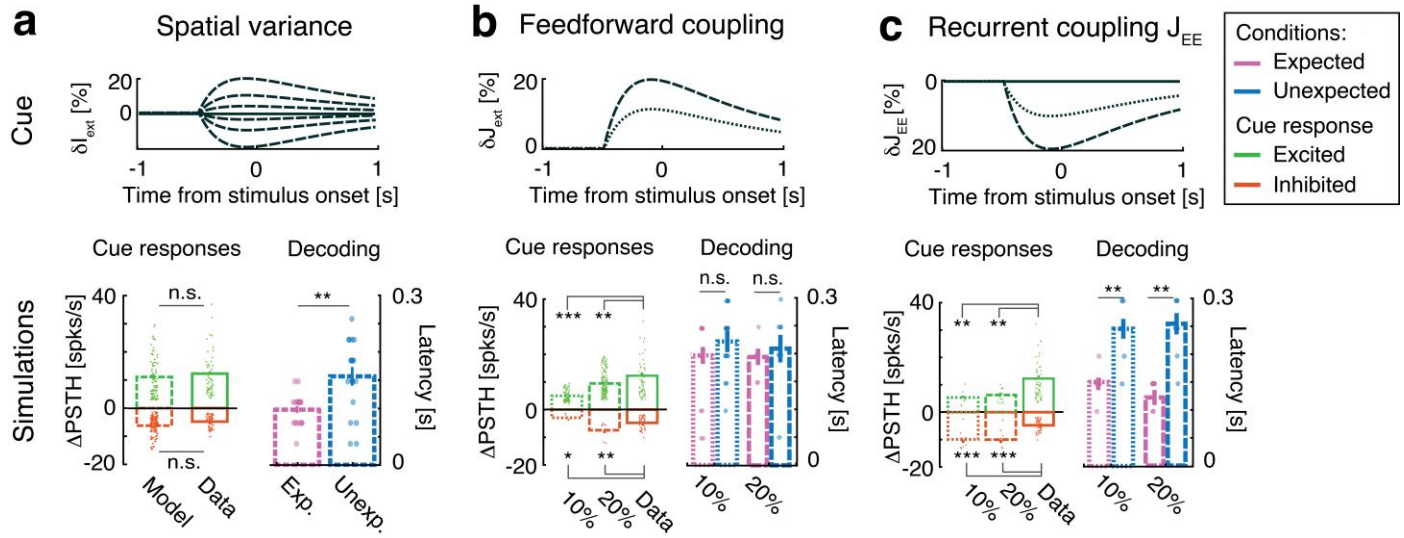

Supplementary Figure 7

Specificity of anticipatory activity (part 1).

We compared our spatial variance model (a, see Fig. 1a-c and Fig. S1a for notations) to alternative models where the anticipatory cue modulates the feedforward couplings J_{ext} (b) or the recurrent couplings J_{EE} (c). All models had the same architecture and cue temporal profile of the main clustered network model (top row panels). In the alternative models, the cue targeted all clustered E neurons. Models were scored on the ability to match the experimental data on typology of cue response and amount of stimulus-coding anticipation. Cue responses were quantified as the ΔPSTH = peak cue response – baseline firing rate as in Fig. S1 (bottom left panels; green: excited neurons, red: inhibited neurons; Δ PSTH, mean ± s.e.m. across neurons from n=10 simulated networks, 50 neurons/network were randomly sampled; dots represent single neurons), while coding anticipation was assessed via latency of stimulus decoding (bottom right panels, notations as in inset of Fig. 1c; aggregate analysis across n=10 simulated networks of the onset times of significant decoding (mean±s.e.m.) in expected (pink) vs. unexpected trials (blue)). In the feedforward coupling model (b), the cue was a time-dependent modulation of the external synaptic coupling $J_{ext} = J_{E0}$, identical for all clustered excitatory neurons. Cue responses were heterogeneous but significantly different from the experimental data (bottom left, two-sided t-test; excited responses: 10% with $p=6.3x10^{-12}$, 20% with $p=4.0x10^{-3}$, inhibited responses: 10% non-significant, 20% with p=0.01); coding anticipation was absent for either moderate or strong positive modulations (10%-20% above baseline; bottom right). For negative cue modulations, only inhibited cue responses were observed and no coding anticipation was present (not shown). In the recurrent coupling model (c), the cue was a time-dependent modulation of the E-to-E recurrent coupling strength J_{EE}. For negative J_{EE} modulation (the more likely to produce a faster dynamics), coding anticipation was present (bottom right, two-sided t-test; 10% with p=0.0039, 20% with p=0.004), however, peak cue responses were strongly inhibited over a wide range of parameters, thus incompatible with the empirical data (bottom left, two-sided t-test; excited responses: 10% with p=0.01, 20% with p=0.0097, inhibited responses: 10% with p=6.9x10-6, 20% with p=2.9x10-6). We obtained similar results after decreasing the spike thresholds of the excitatory neurons (down to -30%, not shown). Increasing the thresholds of inhibitory neurons had no significant impact on the behavior of the model (up to 30%, not shown). For positive J_{EE} modulation (not shown), coding anticipation was absent and cue responses were mostly excited. Non-modulated network parameters were as in Table 1 (all panels). All panels: two-sided t-test, *=p<0.05, **=p<0.01, ***=p<0.001.

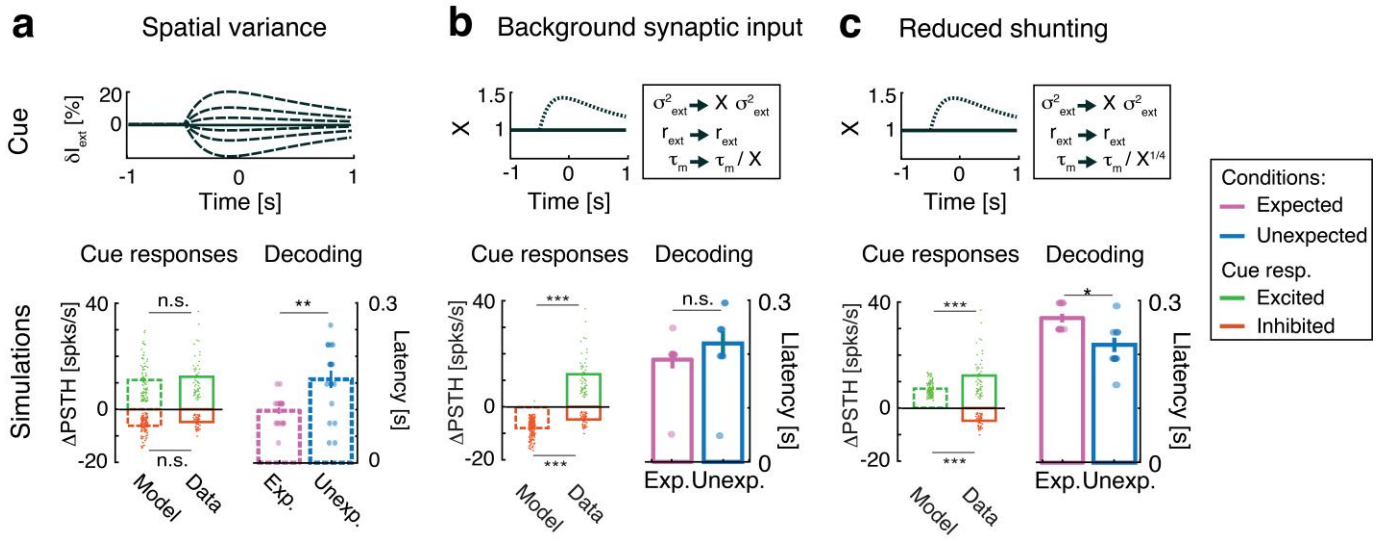

Supplementary Figure 8

Specificity of anticipatory activity (part 2).

We compared our model (**a**, see Fig. 1a-c and Fig. S1a) to an alternative model where the anticipatory cue modulates the *background synaptic input*, driving a simultaneous increase in background noise and shunting inhibition as in Ref[59] (**b**-**c**). The baseline noise level was modeled after an Ornstein-Uhlenbeck process with zero mean and variance $\sigma_{ext} = 0.5\, r_{ext}$, where r_{ext} was the mean afferent current. The cue increased the background noise by a factor X: $\sigma^2_{ext} \rightarrow X\sigma^2_{ext}$ while shunting the membrane time constant by a factor 1/X: $\tau_m \rightarrow \tau_m/X$ (we refer to Ref.[59] for details). Both modulations followed the same double exponential time course of the spatial variance model of the main text (top panels in *b-c*). **b**: With even a moderate factor of X=1.5, the cue induced mostly inhibited cue responses (bottom left panels; green: excited neurons, red: inhibited neurons; ΔPSTH, mean±s.e.m. across neurons from *n=10* simulated networks, 50 neurons/network were randomly sampled; dots represent single neurons), significantly different from the experimental data (two-sided *t*-test; excited responses: n/a; inhibited responses: $p=1.9\text{x}10^{-5}$) and no anticipation (bottom right, aggregate analysis across *n=10* simulated networks of the onset times of significant decoding (mean±s.e.m.) in expected (pink) vs. unexpected trials (blue); two-sided *t*-test, non significant) due to the strong shunting effect on the network dynamics, leading to a strong reduction of excitability in the clusters. At X=2, excitatory neurons were transiently silenced (not shown). **c**: In an effort to obtain a fair comparison with the spatial variance model, we reduced the shunting effect (using peak value τ_m/X^{ϵ}, with X=1.5 and ϵ=1/4) while keeping the same amount of background noise. In this case, cue responses were more similar to the data (two-sided *t*-test; excited responses: $p=1.5\text{x}10^{-7}$; inhibited responses: n/a), but coding slowed down compared to the unexpected condition (bottom right, two-sided *t*-test, *p=0.015*). All panels: two-sided *t*-test, *=p<0.05, **=p<0.01, ***=p<0.001.

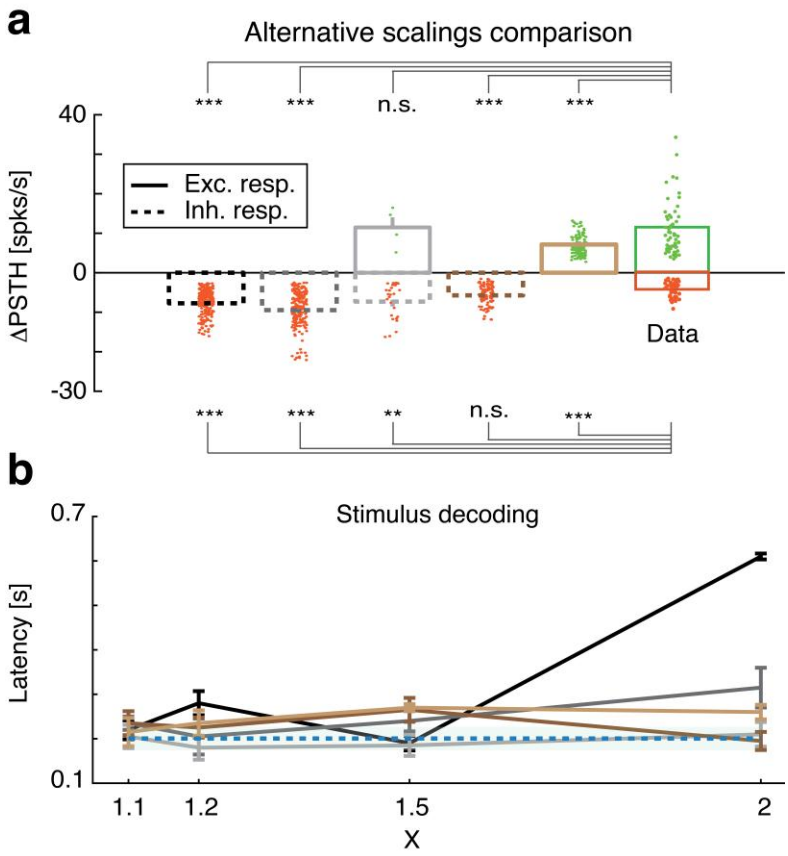

Supplementary Figure 9

Specificity of anticipatory activity (part 3).

In the alternative model where the cue modulates the *background synaptic input* (Fig. S8), we explored the parameter space by independently scaling background noise, shunting, and mean afferent current r_{ext} (transiently increased with the same time course as the other quantities to counteract the shunting effect, see top panels in Fig. S8b-c), but found that coding anticipation was never present (bottom row). We concluded that a model cue inducing an increase in background synaptic activity did not lead to anticipatory activity. **a**: ΔPSTH for X=1.5 (full bar: excited neurons; dashed bar: inhibited neurons; ΔPSTH, mean±s.e.m. across neurons from *n=10* simulated networks, 50 neurons/network were randomly sampled; dots represent neurons with excited (green) and inhibited (red) responses); **b**: decoding latency (aggregate analysis across *n=10* simulated networks of the onset times of significant decoding (mean±s.e.m.) in expected trials; dashed blue line: coding latency in unexpected trials, mean±s.e.m.) as a function of the scaling parameter X for the 5 scaling regimes shown in **a** (same color code). Color code: Black, $\sigma_{ext}^2 \to X\sigma_{ext}^2$, $r_{ext} \to r_{ext}, \tau_m \to \tau_m/X$ (same as in Fig. S8b); Dark grey, $\sigma_{ext}^2 \to X\sigma_{ext}^2$, $r_{ext} \to X^{\frac{1}{2}} r_{ext}, \tau_m \to \tau_m/X$; Light grey, $\sigma_{ext}^2 \to X\sigma_{ext}^2, r_{ext} \to X\, r_{ext}, \tau_m \to \tau_m/X$; Dark brown: $\sigma_{ext}^2 \to X\sigma_{ext}^2$, $r_{ext} \to r_{ext}, \tau_m \to \tau_m/X^{\frac{1}{2}}$; Light brown: $\sigma_{ext}^2 \to X\sigma_{ext}^2$, $r_{ext} \to r_{ext}, \tau_m \to \tau_m/X^{\frac{1}{4}}$ (same as in Fig. S8c). Panel **a**, two-sided *t*-test: *=p<0.05, **=p<0.01, ***=p<0.001.

Supplementary Table S1

	Alternative models			
Modulation	Spatial Var.	Ffwd. (J_{ext})	Rec. (J_{EE})	Backgr. Syn. Input
Anticipation	Yes (robust)	No	Yes	No
Cue responses	Yes (robust)	No	No	Yes (fine tuned)
Figure	S1-S4	S7b	S7c	S8-S9

Comparison of the performance of alternative models of the anticipatory cue. First row ("Modulation") reports the type of modulation due to the cue (feature defining the model as described in captions of Supplementary Figures 7-9). Second row ("Anticipation") reports the presence (Yes) or absence (No) of coding anticipation. Third row ("Cue responses") reports whether the ΔPSTH is compatible (Yes) or not (No) with the empirical data. Last row: Supplementary Figure where the corresponding result is shown.

Supplementary Table S2

Symbol	Description	Value
j_{EE}	Mean E-to-E weights $\times\sqrt{N}$	1.4 mV
j_{EI}	Mean E-to-I weights $\times\sqrt{N}$	5.0 mV
j_{IE}	Mean I-to-E weights $\times\sqrt{N}$	2.5 mV
j_{II}	Mean I-to-I weights $\times\sqrt{N}$	6.1 mV
j_{E0}	Mean afferent synaptic weights to E neurons $\times\sqrt{N}$	7.3 mV
j_{I0}	Mean afferent synaptic weights to I neurons $\times\sqrt{N}$	6.5 mV
J_{+}	Potentiated intra-cluster E-to-E weights factor.	10.5
r^{E}_{ext}	Average afferent rate to E neurons (baseline).	5 spks/s
r^{I}_{ext}	Average afferent rate to I neurons (baseline).	7 spks/s
V^{E}_{thr}	E neuron threshold potential.	3.6 mV
V^{I}_{thr}	I neuron threshold potential.	5.7 mV
V_{reset}	E and I neurons reset potential.	0 mV
τ_m	E and I membrane time constant.	20 ms
τ_{ref}	Absolute refractory period.	5 ms
τ_{syn}	E and I synaptic time constant.	4 ms

Parameters for the network with overlapping clusters with N=2000 LIF neurons (See Supplementary Fig. S5d for details).